QUARTERLY OF APPLIED MATHEMATICS
JANUARY 1983

A THEORY OF ELECTROMAGNETIC INDUCTION IN LAYERED MEDIA: LINEAR MOTOR MODELING*

BY

I. C. RAE

University of St. Andrews

Abstract. A general theory of electromagnetic induction is developed based on the superposition of electric current filaments. The theory has applications in both geophysical and engineering problems where current sources are used to induce electromagnetic fields in plane layered media. As an example, three-dimensional integral formulae are derived for the source and induced fields of a linear induction motor configuration.

1. Introduction. The linear induction motor (l.i.m.) is basically an unwound version of its rotary counterpart [1], but, unlike a rotary motor, the electromagnetic (e.m.) field produced by the current-carrying coils is of finite extent. The applications of an l.i.m. are diverse [2] but its ability to impart motion to adjacent electrical conductors (by inducing a Lorentz body force) without gear mechanisms means that it is extremely useful in driving molten metals, both for the bulk transport of the melt and for induction-stirring [2–6]. In general, a numerical solution (if that is possible) of the nonlinear magnetohydrodynamic equations is necessary in order *fully* to describe the coupling between the flow of the melt and the (three-dimensional) e.m. field produced by the l.i.m. When the flow *weakly* modifies the l.i.m's field, a first approximation for the Lorentz force induced in the melt can be obtained by assuming the melt behaves as a *solid* conductor moving with some *average* velocity (in this case we refer to the conductor as a rotor). The first-order solution for the flow of the melt is then obtained by solving the appropriate hydrodynamic equations [2, 16]. In this paper we derive integral expressions for the first-order e.m. field induced in a rotor by the l.i.m.; the first-order flow is discussed, in part, elsewhere [2].

An example of an l.i.m. is shown in Figure 1a; here, four groups of three coil-wound teeth (identified by the labels R—red, Y—yellow, B—blue) form the source field. Each coil is connected to the same alternating current supply, but the red (blue) coils are phase retarded (advanced) by $2\pi/3$ radians over the yellow coils. If the e.m. field for a *single* coil-wound tooth can be obtained, an l.i.m. can be modeled by superposing suitably placed and phased coils, provided self-inductive effects are negligible. This is the procedure followed here.

The problem posed is therefore one of *electromagnetic induction* by a source placed above layered plane media. The source here is a coil-wound tooth attached to the laminated iron stator core of the l.i.m. (see Figure 1a for the definitions and nomenclature). Its e.m. field can be obtained by superposing current dipole sources over its volume [7],

* Received December 22, 1981.

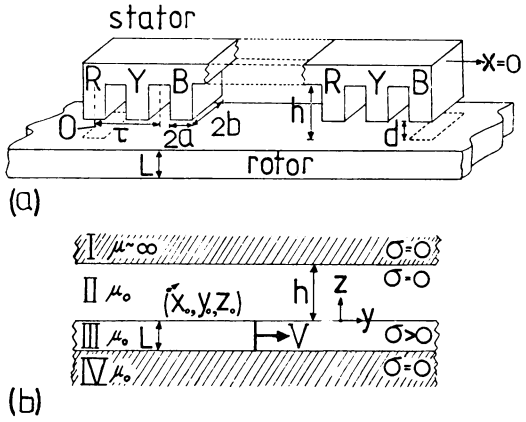

FIG. 1. (a) The linear motor/rotor configuration. Six of the twelve coil-wound teeth are shown—the ordering Red, Yellow, Blue (R, Y, B) is maintained for all twelve teeth; (b) the mathematical model.

taking into account the layered media and iron stator, which modify the free-space solutions. However, the most fundamental building block for a current system is the current filament (see Sec. 2); we use this approach to construct the tooth-field. A general method is derived, based on the current filament, which can be used for the calculation of the induced field of essentially arbitrary sources in multiple-layered plane media of infinite extent. The theory complements the work of Price [8], Gordon [9, 10], Caignard [11] and Weaver [12] but has the advantage that the induced fields are obtained directly, without recourse to free-space source fields. In order not to lose sight of the problem which motivated this research, we present the method entirely within the context of a l.i.m. analysis. An advantage of this approach is that the method follows a natural development and its versatility becomes apparent.

2. The general method.

2.1 *The basic model.* The physical structure to be modeled is shown in Fig. 1a. A rectangular tooth (width 2a, length 2b, height (h − d)) is attached to the underside of a laminated iron core (the stator core); the base of the tooth is placed at a height d above a solid rotor, of thickness L, which moves with the (constant) speed V parallel with the stator face (which lies at a height h above the rotor) in a direction aligned along with the (eventual) axis of the l.i.m.

The mathematical model equivalent to Fig. 1a is shown in Fig. 1b. Cartesian axes are chosen with origin on the surface of the rotor as shown. Denoting electrical conductivity by σ and magnetic permeability by μ, we form four regions: region I ($\sigma = 0$, $\mu \sim \infty$, $z > h$) represents the laminated fully saturated soft iron stator core; region II ($\sigma = 0$, $\mu = \mu_0$, $h > z > 0$) represents the tooth/slot/air gap region; region III ($\sigma \neq 0$, $\mu = \mu_0$, $0 > z > L$) forms the electrically conducting rotor; region IV ($\sigma = 0$, $\mu = \mu_0$, $z < -L$) is an insulating half-space. The magnetic permeability, μ_0, is equal to that of free space. The model extends to infinity in the x and y directions.

The modeling of the tooth is done by superposing elementary current filaments as described in the introduction. One of these current filaments occupies the location $\mathbf{r}_0 = (x_0, y_0, z_0)$ in region II.

2.2 *The basic equations.* The current filament $\mathbf{j}(\mathbf{r}, \mathbf{r}_0) \exp(i\omega t)$ is defined by [13]

$$\mathbf{j}(\mathbf{r}, \mathbf{r}_0) = \mathbf{c}(\mathbf{r}_0)\, \delta(x - x_0)\, \delta(y - y_0)\, \delta(z - z_0). \tag{1}$$

Here, $\mathbf{c} = (c_1, c_2, c_3)$ is a vector ($c_1 = \mathbf{c} \cdot \hat{\mathbf{x}}$, etc.), of dimension equal to current density, defining the *strength* and *direction* of the current filament; $\delta(x)$ is the Dirac delta function; ω is the angular frequency of the winding current. In the quasi-static approximation Maxwell's equations and Ohm's law are linear so we may assume all the electromagnetic variables have the same time variation $\exp(i\omega t)$. Maxwell's equations reduce to

$$\nabla \cdot \mathbf{B} = 0, \nabla \times \mathbf{B} = \mu \mathbf{J}, \qquad \nabla \times \mathbf{E} = -i\omega \mathbf{B}, \qquad \nabla \cdot \mathbf{J} = 0, \qquad \nabla \cdot \mathbf{E} = 0, \tag{2}$$

where $\mathbf{B}(\mathbf{r})$, $\mathbf{E}(\mathbf{r})$ and $\mathbf{J}(\mathbf{r})$ denote the magnetic field, electric field and electric current respectively.

The uniformity of the model in the (x, y)-plane allows the use of the double Fourier transform, defined for $\mathbf{B}(\mathbf{r})$ as

$$\hat{\mathbf{B}}(p, q, z) = \int_{-\infty}^{\infty} \int_{-\infty}^{\infty} \mathbf{B}(\mathbf{r}) \exp(i\mathbf{k} \cdot \mathbf{r})\, dx\, dy, \tag{3}$$

with inverse

$$\mathbf{B}(\mathbf{r}) = \frac{1}{(2\pi)^2} \int_{-\infty}^{\infty} \int_{-\infty}^{\infty} \hat{\mathbf{B}}(p, q, z) \exp(-i\mathbf{k} \cdot \mathbf{r})\, d\mathbf{k}, \tag{4}$$

where $\mathbf{k} = (p, q, 0)$. The transforms of the remaining variables may be similarly defined. Consider now regions II, III and IV and the field structures therein.

Region II: The source current in (1) does not satisfy the conservation law $\nabla \cdot \mathbf{j} = 0$ at $\mathbf{r} = \mathbf{r}_0$. For consistency the scalar current potential $\phi(\mathbf{r}, \mathbf{r}_0)$ is introduced, so that the *total* source current is given by

$$\mathbf{J}(\mathbf{r}, \mathbf{r}_0) = \mathbf{j}(\mathbf{r}, \mathbf{r}_0) - \nabla \phi(\mathbf{r}, \mathbf{r}_0). \tag{5}$$

Since $\nabla \cdot \mathbf{J} = 0$, the function $\phi(\mathbf{r}, \mathbf{r}_0)$ satisfies the Poisson equation

$$\nabla^2 \phi = \nabla \cdot \mathbf{j}. \tag{6}$$

From (2), using (5), the Poisson equation for the magnetic field becomes

$$\nabla^2 \mathbf{B} = -\mu_0 \nabla \times \mathbf{j}. \tag{7}$$

Using the Fourier representation in (3), Eqs. (6) and (7) transform to

$$\left(\frac{d^2}{dz^2} - k^2\right) \hat{\phi} = \left(-ipc_1 - iqc_2 + c_3 \frac{d}{dz}\right) \delta(z - z_0) \exp(i\mathbf{k} \cdot \mathbf{r}_0), \tag{8}$$

$$\left(\frac{d^2}{dz} - k^2\right) \hat{\mathbf{B}} = \left(iqc_3 + c_2 \frac{d}{dz}, -ipc_3 + c_1 \frac{d}{dz}, i(pc_2 - qc_1)\right) \mu_0\, \delta(z - z_0) \exp(i\mathbf{k} \cdot \mathbf{r}_0), \tag{9}$$

where $k^2 = p^2 + q^2$.

Region III: By combining (2) and Ohm's law for a moving medium, $\mathbf{J} = \sigma(\mathbf{E} + \mathbf{V} \times \mathbf{B})$, where $\mathbf{V} = V_y$, the following equation describing the induced fields is easily derived:

$$\left(\nabla^2 - i\omega\mu_0\sigma - \mu_0\sigma V\frac{\partial}{\partial y}\right)\mathbf{B} = 0. \tag{10}$$

By using (2), Eq. (10) may be transformed to

$$\left(\frac{d^2}{dz^2} - \gamma^2\right)\hat{\mathbf{B}} = 0, \tag{11}$$

where

$$\gamma^2 = k^2 + i\mu_0\sigma(\omega - qV). \tag{12}$$

Region IV: Eq. (10) holds with $\sigma = 0$, $V = 0$. In Fourier space we have

$$\left(\frac{d^2}{dz^2} - k^2\right)\hat{\mathbf{B}} = 0. \tag{13}$$

In all three regions $\nabla \cdot \mathbf{B} = 0$ leads to the transformed relation

$$\frac{d\hat{B}_3}{dz} = i(p\hat{B}_1 + q\hat{B}_2). \tag{14}$$

2.3 *Boundary conditions.*

(a) *Physical conditions.* The electromagnetic fields in regions I and IV are assumed to decay for large values of $|z|$. Across $z = 0$ and $z = -L$, $\hat{\mathbf{B}}$ and (from 14)) $d\hat{B}_3/dz$ are continuous. From an analysis of the second of (2) it may be shown that the vertical component of electric current dentisy, J_3, is zero inside the rotor. Physically the current paths lie in the (x, y)-plane; if the rotor is made finite in extent, then $J_3 \neq 0$ in regions close to the perimeter of the rotor, where return currents form. This, together with the electromagnetic boundary condition at the stator core $\mathbf{B} \times \hat{\mathbf{z}} = 0$ (since $\mu \sim \infty$ in region I), yields the condition $\partial\phi/\partial z = 0$ (and so $d\hat{\phi}/dz = 0$) at $z = 0$, $z = h$.

(b) *Continuity conditions.* Consider the differential equation $d^2\theta/dz^2 - \lambda^2\theta = \alpha\,\delta(z - z_0)$ where α and λ are constants. Integrating across $z = z_0$ yields the result that θ is continuous across $z = z_0$, but $d\theta/dz$ is discontinuous by an amount α. The equation $d^2\psi/dz^2 - \lambda^2\psi = \alpha\, d(\delta(z - z_0))/dz$ may be analyzed by writing $\psi = d\theta/dz$, so that ψ is discontinuous by the amount α across $z = z_0$. Writing $F = \exp(i\mathbf{k} \cdot \mathbf{r}_0)$, it is readily shown that the continuity conditions on $\hat{\phi}$, $\hat{\mathbf{B}}$ and their derivatives across $z = z_0$ are as shown in Table 1.

2.4 *Solutions in Fourier space.*

Region II: The solution for $\hat{\phi}$ in (8) may be written

$$\hat{\phi} = \begin{cases} D_1 \cosh k(h - z), & h > z > z_0, \\ D_2 \cosh kz, & z_0 > z > 0, \end{cases} \tag{15}$$

TABLE 1. Discontinuities across $z = z_0$.

Field variable	$\hat{\phi}$	$d\hat{\phi}/dz$	$\hat{B}_1$	$\hat{B}_2$	$d\hat{B}_1/dz$	$d\hat{B}_2/dz$	$d\hat{B}_3/dz$
Discontinuous by	Fc_3	$-iF(pc_2 + qc_3)$	$\mu_0 Fc_2$	$-\mu_0 Fc_1$	$\mu_0 iFqc_3$	$-\mu_0 iFpc_3$	$\mu_0 iF(pc_2 - qc_1)$

since $d\hat{\phi}/dz = 0$ at $z = 0, h$. By applying the continuity conditions across $z = z_0$ (see Table 1) the parameters D_1, D_2 are easily obtained; the solution for $\hat{\phi}$ is

$$\hat{\phi} = F \begin{cases} \dfrac{c_3 \sinh kz_0 \cosh k(h-z)}{\sinh hk} + \dfrac{i(pc_1 + qc_2)\cosh kz_0 \cosh k(h-z)}{k \sinh kh} & h > z > z_0, \\ \dfrac{-c_3 \sinh k(h-z_0)\cosh kz}{\sinh kh} + \dfrac{i(pc_1 + qc_2)\cosh kz \cosh k(h-z_0)}{k \sinh kh} & z_0 > z > 0. \end{cases} \tag{16}$$

The solutions for $\hat{B}_1, \hat{B}_2$ may be written

$$\hat{B}_{1,2} = \begin{cases} L_{1,2} \sinh k(h-z), & z > z_0, \\ M_{1,2} \exp(kz) + N_{1,2} \exp(-kz), & z < z_0. \end{cases} \tag{17}$$

Region III. The solutions for $\hat{B}_1, \hat{B}_2$ are, from (11),

$$\hat{B}_{1,2} = P_{1,2} \exp(\gamma z) + Q_{1,2} \exp(-\gamma z). \tag{18}$$

Region IV: The solutions for $\hat{B}_1, \hat{B}_2$ are, from (13),

$$\hat{B}_{1,2} = R_{1,2} \exp(kz). \tag{19}$$

In each of (17) to (19), $\hat{B}_3$ can be obtained by inspection using (14). The continuity of $\hat{\mathbf{B}}$ and $d\hat{B}_3/dz$ across $z = 0, z = -L$ yields eight equations connecting the twelve parameters of integration above. The remaining four equations required to evaluate the parameters are obtained from the continuity conditions for $\hat{B}_1, \hat{B}_2$ in Table 1. The complete expressions for the integration parameters are given in Appendix I. It is important to note that in regions III and IV, the component c_3 does not occur in the solutions, so *vertical* source currents do not induce currents in the rotor [8]. Note that the fields in region I are not required in this analysis.

For brevity we shall present here only the solution for $\hat{\mathbf{B}}$ in region III (the rotor). We find

$$\begin{pmatrix} \hat{B}_1 \\ \hat{B}_2 \end{pmatrix} = F \begin{pmatrix} p \\ q \end{pmatrix} \frac{\gamma(qc_1 - pc_2)}{k^2 \Delta} \left\{ \left(\frac{\gamma + k}{\gamma - k} \right) e^{2\gamma L} e^{\gamma z} - e^{-\gamma z} \right\} \cosh k(h - z_0), \tag{20}$$

$$\hat{B}_3 = \frac{iF(qc_1 - pc_2}{\Delta} \left\{ \left(\frac{\gamma + k}{\gamma - k} \right) e^{2\gamma L} e^{\gamma z} + e^{-\gamma z} \right\} \cosh k(h - z_0), \tag{21}$$

where

$$\Delta = \left\{ \left(\frac{\gamma + k}{\gamma - k} \right) e^{2\gamma L} - 1 \right\} \gamma \cosh kh + \left\{ \left(\frac{\gamma + k}{\gamma - k} \right) e^{2\gamma L} + 1 \right\} k \sinh kh. \tag{22}$$

The electric current density is given by the transform of the second of (2).

2.5 *Source modeling.* It has already been shown that only the *projection* of the tooth currents onto the rotor has an inducing effect (since c_3 does not occur there). This, of course, does not hold in region II. As far as stator losses are concerned, vertical source currents merely produce ohmic losses and so the stator windings should be layered parallel with the stator face. For simplicity, we therefore let $c_3 = 0$. To illustrate the general procedure to be followed in modeling teeth of any geometry, consider the following examples.

(i) *Line current.* The field solutions in Fourier space all contain the parameter $F = \exp(ipx_0 + iqy_0)$ which arises because the current filament is located at $\mathbf{r} = \mathbf{r}_0$ in real space. If we write $x_0 = u + x_1$, $y_0 = v + y_1$, the position of the current filament in relation to the fixed point (u, v) can be obtained by choosing appropriate values for x_1 and y_1. If the orientation of the element is along the line $y = \alpha x + \beta$ in real space, we may write $\mathbf{c} = (1, \alpha, 0)I\,dx_1$ where dx_1 is a small increment along the x-axis and I is the (here) constant winding current. Combining an infinite number of current filaments along the line $y = \alpha x + \beta$ between (x_2, y_2) and (x_3, y_3) produces a *line current* for which we may define the mapping

$$F(qc_1 - pc_2) \rightarrow Ie^{i(up+vq)}(q - p\alpha) \int_{x_2}^{x_3} e^{i(p+\alpha q)x_1}\,dx_1, \tag{23}$$

where $F(qc_1 - pc_2)$ occurs in (20) and (21).

(ii) *Polygonal coil.* This coil can be modeled by a finite combination of line currents. Summing the formula in (23) for the chosen values of α over the chosen number of line current edges yields the polygonal coil result. For a rectangular coil of length 2b and width 2a, we find

$$F(qc_1 - pc_2) \rightarrow 4ik^2 I \sin(pa) \sin(qb)\, e^{i(up+vq)}/pq. \tag{24}$$

(iii) *Elliptical coils.* To construct an elliptical coil we use the parametric form $(x_0, y_0) = (u, v) + (m \cos\theta, n \sin\theta)$ where the lengths of its semi-major and semi-minor axes are, respectively, m and n. An element of the ellipse is oriented in the direction $\mathbf{c} = I(-n \sin\theta, m \cos\theta, 0)\,d\theta$ (for anti-clockwise current at $t = 0$) where $d\theta$ is a small angle increment. Summing these elements is equivalent to integrating from $\theta = 0$ to $\theta = 2\pi$. For an elliptical current loop we therefore have:

$$F(qc_1 - pc_2) \rightarrow -Ie^{i(up+vq)} \int_0^{2\pi} (nq \sin\theta + mp \cos\theta)\, e^{i(mp\cos\theta + nq\sin\theta)}\,d\theta$$

$$= 2\pi I\psi J_1(\psi)\, e^{i(up+vq)}, \tag{25}$$

where $\psi^2 = m^2p^2 + n^2q^2$ and $J_1(\psi)$ is Bessel's function of order unity. Setting $m = n = r$ in (25) produces the appropriate mapping for a circular coil. Expressions for infinitesimal coils can easily be obtained from (25): for example, with $m = n = r$ and r small, $J_1(\psi) \sim \psi/2$ and, by writing $\pi r^2 I = M$, the magnetic moment of the coil, the mapping for a current dipole is obtained in the limit $r \rightarrow 0$.

The solutions for the fields induced in a conductor by a line current or dipole source, are obtained by substituting (23) to (25) in (20) and (21) using the inversion formula (4). By letting $h \rightarrow \infty$, exact agreement (for $V = 0$) with earlier analyses of e.m. induction by antennae sources [8–12] is found. In general, the Fourier integrals can be evaluated only by asymptotic [14, 15], or numerical methods (which are used here).

To model a rectangular coil wound tooth we use (24) in (20) and (21) and integrate the resulting expressions with respect to z_0 from $z_0 = d$ to $z_0 = h$. For example, the expression for $\hat{B}_3$ in region III becomes

$$\hat{B}_3 = \frac{4kI \sin(pa) \sin(qb) \sinh(k[h-d])}{\Delta} \left\{ \left(\frac{\gamma + k}{\gamma - k} \right) e^{2\gamma L} e^{\gamma z} + e^{-\gamma z} \right\} e^{i(up+vq)}. \tag{26}$$

Hitherto we have assumed that the tooth has rectangular structure, with $c_3 = 0$. Elec-

tric motors are more usually designed with layered windings and therefore the "teeth" become skew and the point $(\bar{x}, \bar{y})$ is a function of z_0; probably $c_3 \neq 0$ as well. This structure is easily incorporated in the solutions (20), (21), etc. The theory therefore allows the analysis of arbitrary tooth structures; for simplicity, however, we consider the simple coil structure in (26).

3. The modeling of a linear induction motor. By using the inverse Fourier transform in (4), the solutions for **B**, **J**, **E** and ϕ may be written as double integrals. In the particular case $V = 0$, Eq. (26) and the equivalent expressions for B_1, B_2 etc., may be reduced to integrals with more well-behaved kernels (see Appendix 2). Remembering that only the real parts of the complex expressions have physical meaning, we write Real $\{B_3 \exp(i\omega t)\} = |B_3| \cos(\omega t + \varepsilon)$, where $B_3 = B_{3,r} + iB_{3,i}$ and $\tan \varepsilon = B_{3,i}/B_{3,r}$ is a real phase quantity. The time-averaged Lorentz body force F induced in the rotor by a (model) coil-wound tooth, is obtained from the formula

$$\mathbf{F} = \tfrac{1}{2} \text{ Real } \{\mathbf{J} \times \mathbf{B}^*\}. \tag{27}$$

The force induced in the rotor by the l.i.m. is found by combining suitably placed and phased (see the introduction) teeth. In this case both **J** and **B** in (27) represent, respectively, the total induced current and magnetic field (due to the twelve coils). For illustration, we consider the particular l.i.m. (Fig. 1a) used in the float-glass process [2, 17] to drive molten tin. If $f(y) \exp(i\omega t)$ represents the behavior of an induced field variable, for fixed x and z, then the l.i.m. induces the field f^M, where

$$f^M(y) = e^{i\theta} \sum_{n=1}^{4} \sum_{m=1}^{3} \alpha_{M+n} f(y + g(c))\, e^{2i(m-1)\pi/3}. \tag{28}$$

In (28), the reference point $y = 0$ is chosen as 0 in Fig. 1a, θ is a parameter specifying the phase of the color group y at $t = 0$, c is the tooth pitch and the function $g(c)$ places each phased tooth in its approximate position. To include the effect of half-wound end teeth (which smooths the end effects [2]) we set $\alpha_{m+n} = 0.5$ ($m + n = 2$ or 7) and $\alpha_{m+n} = 1$ (otherwise). The numerical evaluation (using Gaussian quadrature) of the formulae in Appendix 2 was made with the following parametrization: $a = 5$ cm, $b = 1.3$ cm, $c = 5.1$ cm, $d = 2$ cm, $h = 4.9$ cm, $\sigma = 1.7 \times 10^6$ mhom^{-1}, $\omega = 100\pi$ rad s^{-1}. Extensive discussion of the variation of field quantities with the parameters above is given elsewhere [2]; for brevity we show (in Figs. 2a, b, c) only the time-averaged induced force structure on $z = 0$ (the variation with depth is similar to the usual skin-depth decay). The field quantities have been normalized with respect to the dipole moment $M = 4abI$, so $\mathscr{F} = \mathbf{F}/M^2$. Apart from the non-uniform variation in magnitude (the global maximum and minimum is labeled) of the force components (see also [18, 19]), the most noticeable feature is the presence of an *oscillatory* axial force ($\mathscr{F}_2$). It is apparent that whilst a net axial flow will develop when the l.i.m. is used with a liquid metal secondary conductor, the major part of the induced axial body force causes circulation [2]. The cosine of the phase parameter for the electric current component J_1 is shown in Fig. 2d; in the region of the motor, $\cos \varepsilon$ may be written approximately as $\cos(\alpha y + \nu)$ where ν is a constant and $\alpha = 2\pi/3c$. In fact, this result shows that the current density component (and also the remaining e.m. field components) behave in a *traveling wave* manner, with α as the wavelength of the excitation. More usually, $\alpha = \pi/\tau$ where τ is the pole pitch, so that $\tau = 3c/2$ here (this is consistent with the l.i.m. in Fig. 1a which has eight magnetic poles). The

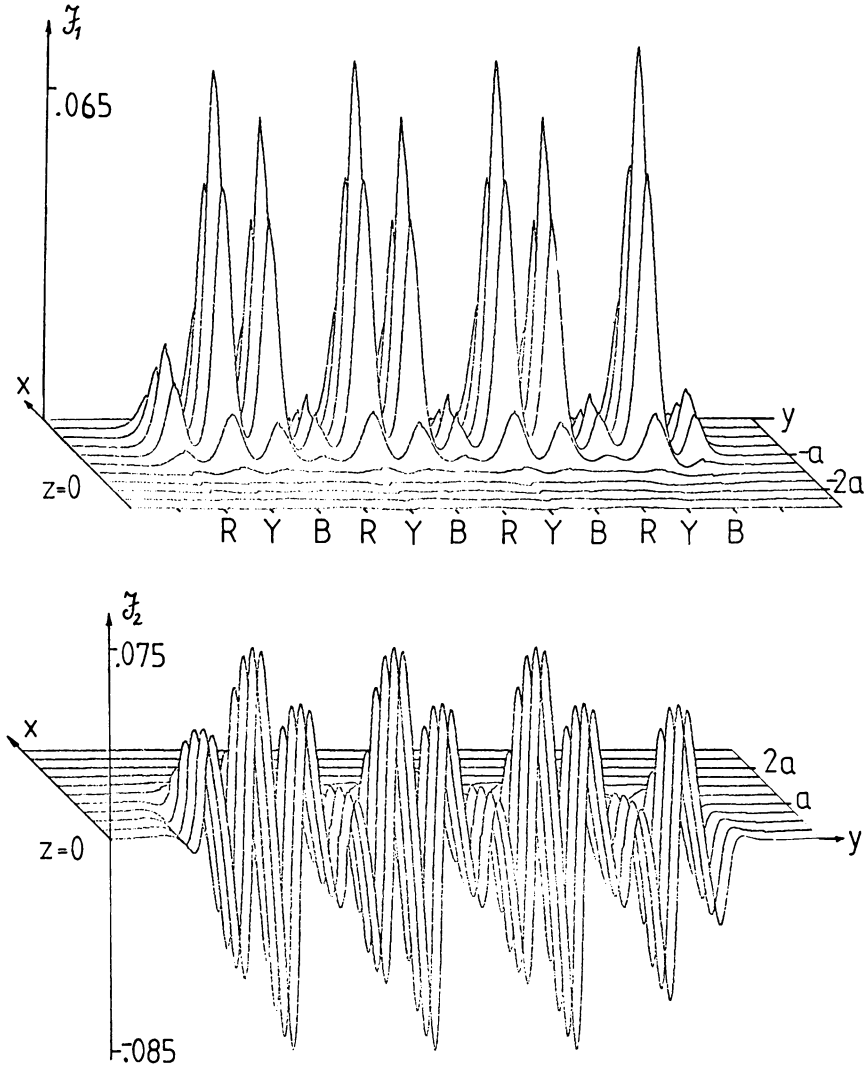

FIG 2. (a) The x-component of the body force; (b) the y-component of the body force; (c) the z-component of the body force; (d) the phase of the x-component of current density.

locations of the phased-teeth in Figs. 2b, c, d follow those in Fig. 2a, but, for clarity, no labeling is made.

In summary, then, we note that apart from the geophysical applications of the general induction method derived earlier, the method has made possible a three-dimensional modeling of both the source and induced l.i.m. fields of an l.i.m. configuration. The usual idealized traveling-wave form for the excitation of a l.i.m. [1, 2] has been vindicated in part; however, it is clear that the local induced flow of a liquid metal secondary can only correctly be discussed using a spatially inhomogeneous model for the l.i.m.

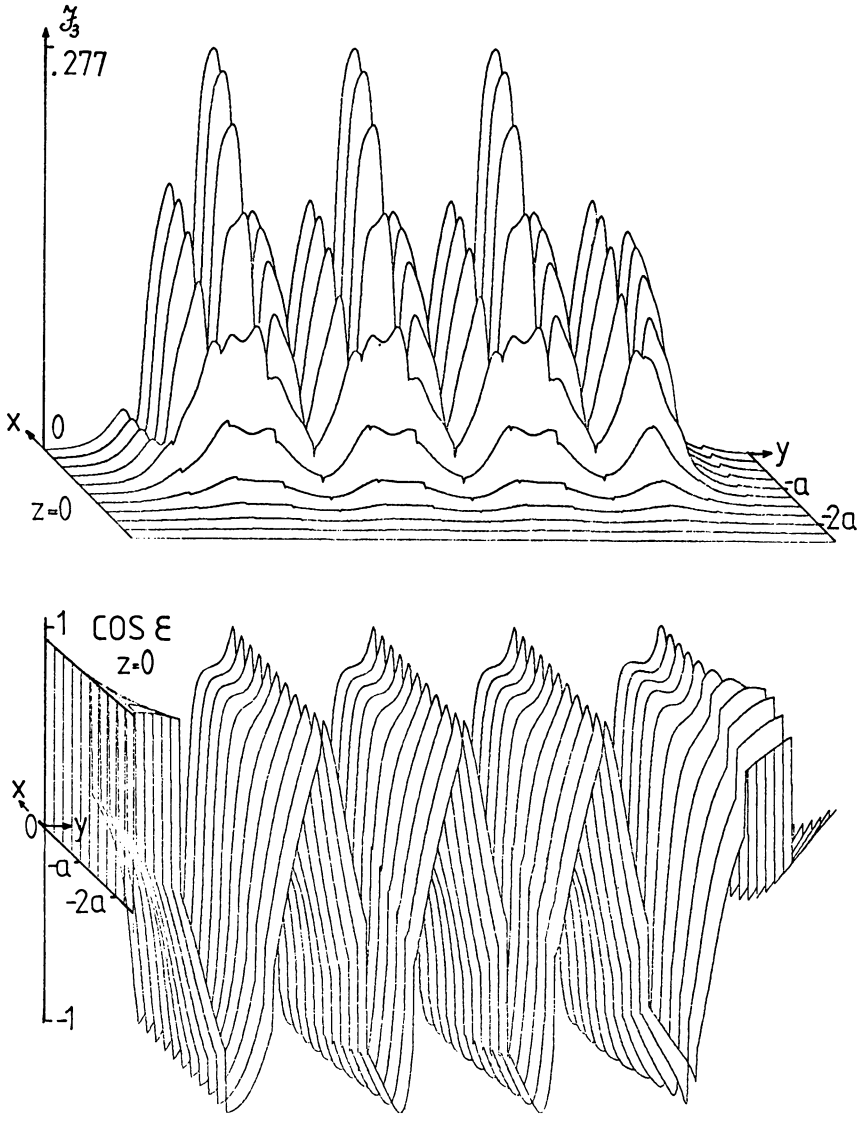

FIG. 2. (Continued)

REFERENCES

[1] E. R. Laithwaite, *Induction machines for special purposes*, Newnes, 1966

[2] I. C. Rae, *Some theoretical problems related to flows induced in liquid metals by linear motors*, Ph.D. thesis, Univ. of Keele, England, 1978

[3] F. R. Block, *Electromagnetic runners and pumps*, ECSC Tech. Res. Rep. EUR 5082 d.e.f., 1973

[4] M. G. Rezin, *Advances in electromagnetic stirring of liquid metals*, Magnitaya Gidrodynamika (2) **1**, 130–138 (1965)

[5] Y. Sundberg, *Magnetic traveling fields for metallurgic purposes*, IEEE Spectrum (5) **6**, 79–88 (1969)
[6] L. R. Blake, *Conduction and induction pumps for liquid metals*, Proc. IEE (A) **4**, 49–63 (1956)
[7] V. C. A. Ferraro, *Electromagnetic theory*, Athlone, 1954
[8] A. T. Price, *Electromagnetic induction in a semi-infinite conductor with a plane boundary*, Q. J. Mech. Appl. Math. **3**, 385–410 (1950)
[9] A. N. Gordon, *The field induced by an oscillating magnetic dipole outside a semi-infinite conductor*, Q. J. Mech. Appl. Math. **4**, 106–115 (1951)
[10] A. N. Gordon, *Electromagnetic induction in a uniform semi-infinite conductor*, Q. J. Mech. Appl. Math. **4**, 116–128 (1951)
[11] L. Cagniard, *Basic theory of the magneto-telluric method of geophysical prospecting*, Geophysics **18**, 605–635 (1953)
[12] J. T. Weaver, *The general theory of electromagnetic induction in a conducting half space*, Geophys. J. R. Astr. Soc. **22**, 83–100 (1970)
[13] P. C. Clemmow and J. P. Dougherty, *Electrodynamics of particles and plasmas*, Addison-Wesley 1969
[14] J. T. Weaver and D. J. Thompson, *The field induced in a two-layer conductor by a magnetic dipole*, Can. J. Physics **48**, 71–79 (1970)
[15] J. R. Wait, *The magnetic dipole over the horizontally stratified earth*, Can. J. Physics **29**, 577–592 (1951)
[16] I. C. Rae, *On the flow induced in liquid metals by a linear induction motor*, App. Sci. Res. **39**, 71–81 (1982)
[17] L. A. B. Pilkington, *The float glass process*, Proc. Roy. Soc. Lond. (A) **314**, 1–25 (1969)
[18] K. Oberretl, *Dreidimensionale Berechnung des linear Motors mit Berucksichtigung der Endefekte und der Wicklungoverteilung*, Arch. fur Elect. **55**, 181–190 (1973)
[19] O. A. Gerasev, Yu. I. Koskin and L. A. Tseitlin, *A three-dimensional model of a linear synchronous motor (theory and calculation)*, Izv. Akad. Nank. SSSR. Energ. Transport (2) **17**, 49–60 (1979)

Appendix 1. The constants of integration are as follows:

$$\begin{Bmatrix} L_1 \\ L_2 \end{Bmatrix} = F\left(\begin{Bmatrix} c_2 \\ -c_1 \end{Bmatrix} \cosh kz_0 + \begin{Bmatrix} -q \\ p \end{Bmatrix} \frac{ic_3 \sinh kz_0}{k} - \gamma \cosh k(h - z_0)\right.$$
$$\left. \times \begin{Bmatrix} p \\ q \end{Bmatrix} \frac{(qc_1 - pc_2)}{k^2\Delta}\left[1 - \left(\frac{\gamma + k}{\gamma - k}\right) e^{2\gamma L}\right]\right) \Big/ \sinh kh,$$

$$\begin{Bmatrix} M_1 \\ M_2 \end{Bmatrix} = F\left(\begin{Bmatrix} -c_2 \\ c_1 \end{Bmatrix} \cosh k(h - z_0) + \begin{Bmatrix} -q \\ p \end{Bmatrix} \frac{ic_3 \sinh k(h - z_0)}{k}\right.$$
$$\left. + \begin{Bmatrix} p \\ q \end{Bmatrix} \frac{\gamma \sinh k(h - z_0)(qc_1 - pc_2)}{k^2\Delta}\left[1 - \left(\frac{\gamma + k}{\gamma - k}\right) e^{2\gamma L}\right] e^{-kh}\right) \Big/ 2 \sinh kh,$$

$$\begin{Bmatrix} N_1 \\ N_2 \end{Bmatrix} = F\left(\begin{Bmatrix} c_2 \\ -c_1 \end{Bmatrix} \cosh k(h - z_0) + \begin{Bmatrix} q \\ -p \end{Bmatrix} \frac{ic_3 \sinh k(h - z_0)}{k}\right.$$
$$\left. + \begin{Bmatrix} p \\ q \end{Bmatrix} \frac{(\gamma \sinh k(h - z_0)(qc_1 - pc_2)}{k^2\Delta}\left[1 - \left(\frac{\gamma + k}{\gamma - k}\right) e^{2\gamma L}\right] e^{kh}\right) \Big/ 2 \sinh kh,$$

$$\begin{Bmatrix} P_1 \\ P_2 \end{Bmatrix} = F \begin{Bmatrix} p \\ q \end{Bmatrix} \frac{(\gamma + k)\gamma(qc_1 - pc_2)\, e^{2\gamma L} \cosh k(h - z_0)}{k^2(\gamma - k)\Delta},$$

$$\begin{Bmatrix} Q_1 \\ Q_2 \end{Bmatrix} = F \begin{Bmatrix} -p \\ -q \end{Bmatrix} \frac{\gamma(qc_1 - pc_2) \cosh k(h - z_0)}{k^2\Delta},$$

$$R_{1,2} = e^{+kL}(P_{1,2}\, e^{-\gamma L} + Q_{1,2}\, e^{\gamma L}).$$

Appendix 2. The integral expressions for the induced (region III) magnetic induction and electric current density (with $V = 0$) are:

$$\begin{Bmatrix} B_1 \\ B_2 \end{Bmatrix} = M \int_0^\infty \frac{\gamma \sinh k(h-d)k^2}{\Delta} \left[\left(\frac{\gamma + k}{\gamma - k} \right) e^{2\gamma L} e^{\gamma z} - e^{-\gamma z} \right]$$

$$\times \begin{Bmatrix} \int_{v=-b}^{v=b} \\ \int_{u=-a}^{u=a} \end{Bmatrix} [J_0(k\rho_{1,2}^+) - J_0(k\rho_{1,2}^-)] \begin{Bmatrix} dv \\ du \end{Bmatrix} dk,$$

$$B_3 = -M \int_0^\infty \frac{\sinh k(h-d)k^3}{\Delta} \left[\left(\frac{\gamma + k}{\gamma - k} \right) e^{2\gamma L} e^{\gamma z} + e^{-\gamma z} \right]$$

$$\times \int_{u=-a}^{u=a} \int_{v=-b}^{v=b} J_0(k\rho)\, du\, dv\, dk,$$

$$\mu_0 \begin{Bmatrix} J_1 \\ J_2 \end{Bmatrix} = \frac{M\omega L^2}{\eta} \int_0^\infty \frac{\sinh k(h-d)k^2}{\Delta} \left[\left(\frac{\gamma + k}{\gamma - k} \right) e^{2\gamma L} e^{\gamma z} + e^{-\gamma z} \right]$$

$$\times \begin{Bmatrix} -\int_{u=-a}^{u=a} \\ \int_{v=-b}^{v=b} \end{Bmatrix} [J_0(k\rho_{2,1}^+) - J_0(k\rho_{2,1}^-)] \begin{Bmatrix} du \\ dv \end{Bmatrix} dk,$$

where

$$\rho^2 = (u-x)^2 + (v-y)^2, \qquad (\rho_1^\pm)^2 = (a \mp x)^2 + (v-y)^2, \qquad (\rho_2^\pm)^2 = (v-x)^2 + (b \mp y)^2,$$

and the transformation

$$\int_{-\infty}^{\infty} \int_{-\infty}^{\infty} F(k)\, e^{-i(px+qy)}\, dp\, dq = 2\pi \int_0^\infty kF(k) J_0(k\sqrt{x^2+y^2})\, dk$$

has been employed in deriving **B**, **J** above.